

Phonon anomalies in α -uranium

Xiaodong Yang and Peter S. Riseborough
Physics Department, Temple University, USA

(Received 15 July 2010; revised manuscript received 6 August 2010)

The phonon spectrum of α -uranium has been measured by Manley *et al.* in a series of experiments using inelastic neutron and x-ray scattering. The 2001 results showed that the optic modes soften by a few millielectron volts as the temperature is increased between room temperature and 450 K. In 2006, a new dynamical mode was observed to form above 450 K which the authors attribute to an intrinsically localized mode, which stabilized by anharmonic interactions. We propose a possible alternate cause for the formation of the mode and the softening which is based on the existence of strong electron-phonon interaction together with a low excitation energy for transitions between states with f and conduction-electron characters. The model allows for a resonant interaction between the optic phonons and the electronic excitations, which may lead to the high-energy peaks in the phonon spectra splitting and acquiring mixed electronic and phonon characters.

DOI: XXXX

PACS number(s): 63.20.kd, 73.20.Mf

I. INTRODUCTION

Uranium shows indisputable evidence for very strong electron-phonon coupling¹ which is responsible for the material undergoing three structural transformations at low temperatures. The room-temperature phonon-dispersion relations inferred from inelastic neutron-scattering experiments² show the existence of a large Kohn anomaly near $q=[0.5, 0, 0]$ in reciprocal-lattice units. The anomaly has its origin in a weak singularity in the dielectric constant at $q=2k_F$.³ Although this singularity is extremely weak for isotropic three-dimensional materials, it can be large for systems in which the electronic dispersion relations are extremely anisotropic. From neutron-diffraction data it was found^{4,5} that on decreasing temperature new inelastic Bragg peaks first occurred for temperatures below 46 K at points near $[\frac{1}{2}, 0, 0]$ which are not commensurate with the α -phase lattice. Also additional peaks were observed at large wave vectors. Yamada⁶ proposed a quasi-one-dimensional theory in which the instability occurs due to Fermi-surface nesting at a wave vector directed along the $[1, 0, 0]$ axis, and that the extra peaks were consequences of strains induced by domain-wall boundaries. However, it was subsequently found using high-resolution neutron scattering⁷ that phonon softening occurred at the exact (temperature-dependent) charge-density wave vectors $Q_c(T)$ off the $[1, 0, 0]$ axis, and that the square of the soft-mode frequency exhibited a linear variation in $T-T_c$ as expected from the mean-field version of Landau-Ginzberg Theory. The wave vectors Q_c were found to be in perfect agreement with the nesting wave vectors of a fully three-dimensional Fermi surface calculated by Fast *et al.*⁸ First-principles calculations of the phonon spectrum by Bouchet⁹ show that the Σ_4 mode shows a significant Kohn anomaly at $[\frac{1}{2}, 0, 0]$. The shift of the phonon frequency can be expressed in terms of a product involving the electron-phonon interaction and the linear-response function for electronic excitations. The magnitude of the shift is surprisingly large since only a relatively small portion of the Brillouin zone shows nesting⁸ and, furthermore, even in these small regions there is about a 5% variation in the nesting vector. Therefore, the Lindhardt function is not expected to show the $\ln(q_x - Q_c)$

divergence expected from perfectly parallel sheets of the Fermi surface but also, at finite values of $(q_x - Q_c)$, is expected to have a magnitude much smaller than the value of the corresponding one-dimensional function. These findings not only suggest that the lattice instability due to the phonon softening can be thought as a Kohn anomaly produced by the electron-phonon interaction and provides a direct measure of the Fermi-surface nesting¹⁰ but also that the electron-phonon interaction is quite strong.

The thermodynamic properties of α -uranium are also anomalous. The lattice constant shows an unusually large temperature dependence that persists up to room temperatures.¹¹ Likewise, the magnetic susceptibility, which has been designated as being Pauli paramagnetic,¹² shows an increase with increasing temperature. Taken together, the thermodynamics suggests that there is a low-energy scale for electronic excitations which results in a decrease in bonding and an increase in the magnetic character at elevated temperatures. Therefore, studies of the high-temperature properties could be expected to reveal distinct physics.

The dispersion relation has also been measured at high temperatures ($T \approx 450$ K) by inelastic neutron and x-ray scattering experiments.^{13,14} These experiments showed that the optic phonon density of states measured by incoherent inelastic neutron scattering softened by about 4 meV as the temperature was raised from room temperature to 433 K. More surprisingly, further experiments revealed the formation of a dynamical mode with a nontrivial temperature-dependent width.¹⁵ The new mode was observed at 14 meV near the zone boundary at the low-symmetry point $(0, 1, 0.2)$, where the pre-existing phonon mode at 11 meV was observed to soften. Further experiments¹⁶ have shown that the anomalous mode occurs at a number of low-symmetry points which are related by an approximate hexagonal symmetry of the Brillouin zone. Since the system does not show signs of a structural instability in the temperature range where the new mode forms, the occurrence of the new mode has been heralded as representing a breakdown of harmonic phonon theory, which would predict six phonon modes for a monoclinic lattice with two basis atoms. (The lattice is normally referred to as orthorhombic with four atoms in the unit cell).

97 The experimental group attributed the appearance of the
 98 new mode to the existence of a thermally activated popula-
 99 tion of intrinsically localized modes. Loosely speaking, in-
 100 trinsically localized modes are oscillatory vibrational modes
 101 in which the anharmonic interactions restrict the excitations
 102 to occur over finite regions of space and which prevent the
 103 excitations from dispersing as time evolves. Evidence for
 104 such nonlinear excitations were first found by Fermi *et al.*¹⁷
 105 in computer simulations of the vibrational motion of a 33-
 106 atom chain in which anharmonic interactions were present.
 107 The continuum limit of the Fermi-Pasta-Ulam problem was
 108 identified as being governed by the Korteweg-de Vries
 109 equation¹⁸ which was shown by Gardner *et al.*¹⁹ to have
 110 soliton solutions. Further progress was made by Toda,²⁰ who
 111 found nonlinear excitations in discrete one-dimensional lat-
 112 tices. Flach²¹ showed that localized large-amplitude vibra-
 113 tional modes can be considered as quantized bound states of
 114 extended small-amplitude waves. Most of the earlier work
 115 has been restricted to low-dimensional systems due to Der-
 116 rick's theorem which predicts that solitonlike modes would
 117 become unstable in higher dimensions.²² Although exact
 118 soliton and breather solutions occur frequently for low-
 119 dimensional nonlinear systems,^{23,24} it has proved to be noto-
 120 riously difficult to obtain mathematically exact soliton solu-
 121 tions for higher dimensional nonlinear theories. However, the
 122 theorem is based on idealized mathematical assumptions and
 123 does not preclude the existence of metastable nonlinear lo-
 124 calized modes. Hence, as Manley *et al.*¹⁵ argue, intrinsically
 125 localized modes might exist in higher dimensions due to "hot
 126 spots" and also in discrete lattices which have relatively low
 127 point-group symmetries such as α -uranium. The experimen-
 128 tal work on α -uranium was followed up by inelastic neutron-
 129 scattering experiments on NaI,²⁵ which showed features con-
 130 sistent with the intrinsically localized modes predicted by
 131 classical molecular-dynamics simulations.²⁶ A thorough dis-
 132 cussion of the appearance of intrinsically localized modes in
 133 three-dimensional materials, including their effects on the
 134 mechanical properties, is given in a recent article by
 135 Manley.²⁷

136 At ambient conditions, the electronic structure of
 137 α -uranium is reasonably well described by density-
 138 functional theory^{28,29} which is in qualitative agreement with
 139 photoemission³⁰ and de Haas-van Alphen experiments.³¹
 140 However, local-density approximation (LDA) does require
 141 some corrections¹ due to moderate correlations given by a
 142 GW treatment.³² As pointed out by Hjelm *et al.*³³ and also by
 143 Stojic *et al.*,³⁴ a modest increase in the unit-cell volume
 144 makes α -uranium comparable to plutonium. For the ex-
 145 panded lattice, LDA predicts α -uranium to be magnetic.
 146 Likewise, LDA predicts plutonium to be magnetic.^{35,36} How-
 147 ever, experiments on plutonium have shown that it does not
 148 possess a spontaneous magnetic moment,³⁷ which is prob-
 149 ably due to a partial cancellation between the spin and orbital
 150 moments³⁸ and also due to valence fluctuations.³⁹ Anomalies
 151 in the phonon spectrum of plutonium were predicted on the
 152 basis of the coupling to low-energy electronic excitations
 153 within the dynamical mean-field theory⁴⁰ and have subse-
 154 quently been observed by inelastic x-ray scattering.⁴¹ The
 155 properties of the actinide materials, including uranium and
 156 plutonium have recently been reviewed by Moore and van

der Laan.⁴² Since the α -uranium lattice expands significantly
 as the temperature increases, one could expect that the mod-
 erate many-body effects predicted near $T=0$ should become
 significantly stronger at temperatures on the order of 450 K.
 The anomalous phonon spectrum of plutonium motivates the
 investigation of whether the phonon anomalies observed in
 the high temperature expanded lattice of α -uranium could
 also be due to coupling with low-energy electronic excita-
 tions. In the next section, we shall present a model for the
 phonon softening which involves strong electron-phonon
 coupling and low-energy valence fluctuations.^{43,44} In the fol-
 lowing section the phonon spectrum will be calculated and
 then the paper will conclude with a discussion of the results
 and a comparison with the experimental data.

II. MODEL HAMILTONIAN

The model Hamiltonian is based on the noninteracting
 Anderson lattice model which describes hybridized $5f$ bands
 and the conduction bands. The harmonic phonons are
 coupled to the f electronic system via an electron-phonon
 interaction. The model was originally introduced by Sher-
 ington *et al.*^{45,46} to describe the dynamics of isostructural
 valence transitions in SmS, where the transition is marked by
 a discontinuous change in volume caused by the differences
 in the ionic radii of the Sm ions. The total Hamiltonian is
 written as

$$\hat{H} = \sum_{i,\sigma} E_f f_{i\sigma}^\dagger f_{i\sigma} + \sum_{k,\sigma} \epsilon_k d_{k\sigma}^\dagger d_{k\sigma} + \sum_{k,\sigma} (V_k f_{k\sigma}^\dagger d_{k\sigma} + V_k^* d_{k\sigma}^\dagger f_{k\sigma}) \\ + \sum_{q,\gamma} \hbar \omega_{q\gamma} a_{q\gamma}^\dagger a_{q\gamma} + \sum_{k,\sigma,q,\gamma} \lambda_{q\gamma} (a_{q\gamma}^\dagger + a_{-q\gamma}) f_{k+q\sigma}^\dagger f_{k\sigma}. \quad (1)$$

The first term represents the binding energy E_f of the local-
 ized f states at the lattice sites labeled by the index i . Here
 the operators $f_{i\sigma}^\dagger$ and $f_{i\sigma}$, respectively, create and annihilate
 an f electron of spin σ in the orbital located at site i . The
 second term represents the energy ϵ_k of the conduction-band
 Bloch states, labeled by the Bloch wave vector k , and $d_{k\sigma}^\dagger$
 and $d_{k\sigma}$, respectively, create and annihilate a conduction elec-
 tron of spin σ in the k th Bloch state. The third term repre-
 sents the hybridization between the localized f electron states
 and the conduction-band states. The fourth term represents
 the energy $\hbar \omega_{q\gamma}$ of a phonon with wave vector q and polar-
 ization γ in which $a_{q\gamma}^\dagger$ and $a_{q\gamma}$ are, respectively, the phonon
 creation and annihilation operators. The last term represents
 the interaction between the f electron and the phonons. The
 order of magnitude of the f electron-phonon coupling
 strength $\lambda_{q,\gamma}$ for longitudinal-acoustic phonons is approxi-
 mated by⁴⁷

$$\lambda_q = i(q \cdot \epsilon_q) \left[\frac{4\pi Z_* e^2}{\Omega_c (q^2 + q_{TF}^2)} \right] \sqrt{\frac{\hbar}{2M\omega_q}}, \quad (2)$$

where ϵ_q is the polarization vector, Z_* is the charge on the
 uranium ions ($Z_*=3$), M the nuclear mass ($M=238m_p$), Ω_c is
 the volume of the unit cell ($\Omega_c=83.2 \times 10^{-30}$ m³ for the con-
 ventional orthorhombic unit cell), and q_{TF} is the Thomas-

206 Fermi wave vector. The corresponding expression for the
207 longitudinal-acoustic phonon frequency is given by

$$\omega_q^2 = \frac{16\pi Z_*^2 e^2}{M\Omega_c} \left(\frac{q^2}{q^2 + q_{TF}^2} \right). \quad (3)$$

208

209 This results in the energy of the longitudinal phonon at q
210 $= (0, 0, \pi/c)$ to be approximately 18 meV. Although the
211 longitudinal-acoustic and transverse-optic modes do mix
212 slightly yielding a pair of Λ_1 modes, the experimentally de-
213 termined zone-boundary phonon with an energy of approxi-
214 mately 12 meV does correspond to a longitudinal-acoustic
215 mode. The magnitude of the electron-phonon interaction cor-
216 responding to the zone-boundary longitudinal-acoustic mode
217 is found to be approximately 110 meV. A similarly large
218 estimate of the electron-phonon interaction (≈ 47 meV) can
219 be inferred from consideration of the contraction of the
220 Wigner-Seitz radius along the actinide series, as for example,
221 shown in the paper by Lashley *et al.*³⁷ These large values
222 could also be anticipated from analysis of the low-
223 temperature phonon softening which gives rise to structural
224 instabilities. In our analysis, we shall find it necessary to use
225 electron-phonon interactions which have magnitudes that are
226 similar to the phonon energies. The conduction-band width
227 W found from the calculations of Chantis *et al.*³² is estimated
228 to be on the order of 6 eV. The Fermi energy is assumed to
229 lie close to the position of the peak in the density of states of
230 the upper hybridized band. A value of the hybridization ma-
231 trix element V of about 1/3 eV would be required to obtain
232 reasonable agreement with the density of states at the Fermi
233 energy found from the electronic-structure calculations.

234 In the limit where the electrons are noninteracting, i.e.,
235 $\lambda_{q,\gamma} = 0$, the electronic structure decouples from the phonons.

236 The electronic part of the noninteracting Hamiltonian \hat{H}_0 is
237 given by

$$\hat{H}_0 = \sum_{k,\sigma} (E_{fj} f_{k\sigma}^\dagger f_{k\sigma} + \epsilon_k d_{k\sigma}^\dagger d_{k\sigma} + V_{kj} f_{k\sigma}^\dagger d_{i\sigma} + V_k^* d_{k\sigma}^\dagger f_{k\sigma}), \quad (4)$$

238

239 which is diagonal in the Bloch index. The phase of the hy-
240 bridization matrix elements can be gaged away by absorbing
241 the phase in either the d or f electron operators. The nonin-
242 teracting Hamiltonian can then be diagonalized by introduc-
243 ing a pair of new fermionic operators α_k, β_k , via the canoni-
244 cal transformation

$$\begin{aligned} \alpha_{k\sigma} &= f_{k\sigma} \cos \Theta_k + d_{k\sigma} \sin \Theta_k, \\ \beta_{k\sigma} &= -f_{k\sigma} \sin \Theta_k + d_{k\sigma} \cos \Theta_k, \end{aligned} \quad (5)$$

247 where Θ_k is still to be determined. Since the transformation
248 is canonical, the new fermion operators satisfy the anticom-
249 mutation relations,

$$\begin{aligned} \{\alpha_{k\sigma}, \alpha_{k'\sigma'}^\dagger\}_+ &= \delta_{kk'} \delta_{\sigma\sigma'}, \\ \{\beta_{k\sigma}, \beta_{k'\sigma'}^\dagger\}_+ &= \delta_{kk'} \delta_{\sigma\sigma'}, \\ \{\alpha_{k\sigma}, \beta_{k'\sigma'}^\dagger\}_+ &= 0. \end{aligned} \quad (6)$$

253 For the choice of Θ_k given by

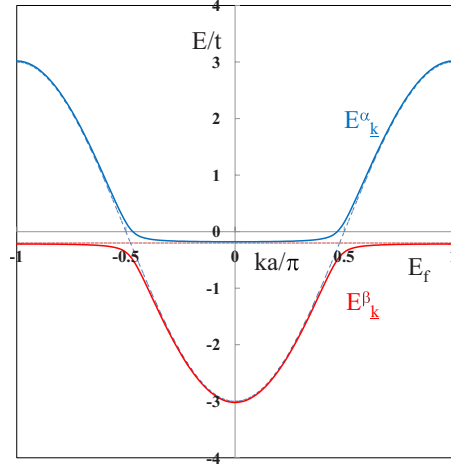


FIG. 1. (Color online) A sketch of the dispersion relations for the hybridized electronic bands.

$$\cos 2\Theta_k = \frac{E_f - \epsilon_k}{\sqrt{(E_f - \epsilon_k)^2 + 4V_k^2}}, \quad (7)$$

$$\sin 2\Theta_k = \frac{2V_k}{\sqrt{(E_f - \epsilon_k)^2 + 4V_k^2}}, \quad (7)$$

the terms in the Hamiltonian which are bilinear in the fermion operators α and β vanish. For this choice, the noninteracting electronic Hamiltonian has the diagonal form

$$\begin{aligned} \hat{H}_0 &= \sum_{k,\sigma} \left(\frac{E_f + \epsilon_k}{2} + \sqrt{\left(\frac{E_f - \epsilon_k}{2} \right)^2 + V_k^2} \right) \alpha_{k\sigma}^\dagger \alpha_{k\sigma} \\ &+ \sum_{k,\sigma} \left(\frac{E_f + \epsilon_k}{2} - \sqrt{\left(\frac{E_f - \epsilon_k}{2} \right)^2 + V_k^2} \right) \beta_{k\sigma}^\dagger \beta_{k\sigma}. \end{aligned} \quad (8)$$

The electronic dispersion relations are shown in Fig. 1. We note that the spectrum exhibits a direct gap between the pair of hybridized bands of $2V$ and an indirect gap given by $\Delta = \frac{4V^2}{W}$, where W is the conduction-band width.

The electron-phonon interaction Hamiltonian \hat{H}_1 can be rewritten in terms of the hybridized states as

$$\begin{aligned} \hat{H}_1 &= \frac{1}{\sqrt{N}} \sum_{k,q,\sigma,\gamma} \lambda_{q,\gamma} (a_{q\gamma}^\dagger + a_{-q\gamma}) (\alpha_{k\sigma}^\dagger \alpha_{k-q\sigma} \cos \Theta_k \cos \Theta_{k-q} \\ &+ \beta_{k\sigma}^\dagger \beta_{k-q\sigma} \sin \Theta_k \sin \Theta_{k-q} - \alpha_{k\sigma}^\dagger \beta_{k-q\sigma} \cos \Theta_k \sin \Theta_{k-q} \\ &- \beta_{k\sigma}^\dagger \alpha_{k-q\sigma} \sin \Theta_{k-q} \cos \Theta_k), \end{aligned} \quad (9)$$

where the coherence factors project onto the f states. In the next section, the phonon spectrum will be calculated using a perturbation expansion in the electron-phonon interaction.

III. PHONON SPECTRA

In the absence of interactions, the phonon propagator $D_{q\gamma}^0(\omega)$ is diagonal in the polarization indices γ is given by

$$D_{q\gamma}^0(\omega) = \frac{2\hbar\omega_{q\gamma}}{\hbar^2\omega^2 - \hbar^2\omega_{q\gamma}^2}. \quad (10)$$

$$\text{Im } \Pi_q(\omega + i\eta) = -\frac{Pr}{\pi} \int_{-\infty}^{+\infty} d\omega' \frac{\text{Re } \Pi_q(\omega')}{\omega' - \omega - i\eta}, \quad (16)$$

276

277 The propagator for the interacting phonons $D_q(\omega)$ can be
278 expressed in terms of the noninteracting propagator and the
279 irreducible polarization part, $\Pi_q(\omega)$, via Dyson's equation

$$D_q(\omega) = D_q^0(\omega) + D_q^0(\omega)\Pi_q(\omega)D_q(\omega). \quad (11)$$

281 To lowest order in the electron-phonon interaction, the irre-
282 ducible polarization part is given by

$$\Pi_q(\omega) = \frac{\hbar}{N} \sum_{k,\sigma} \int \frac{d\omega'}{2\pi i} |\lambda_{q,\gamma}|^2 G_{k+q,\sigma}^0(\omega' + \omega) G_{k,\sigma}^0(\omega'), \quad (12)$$

283

284 where $G_{k,\sigma}^0(\omega)$ is the noninteracting single-particle f -electron
285 Green's function. On evaluating the integrations, one obtains
286 the real part of the polarization part as

$$\begin{aligned} \text{Re } \Pi_q(\omega) = & \frac{2\lambda_{q,\gamma}^2}{N} \sum_k \left[\frac{(f_k^\alpha - f_{k+q}^\alpha) \cos^2 \Theta_k \cos^2 \Theta_{k+q}}{\hbar\omega + E_k^\alpha - E_{k+q}^\alpha} \right. \\ & + \frac{(f_k^\beta - f_{k+q}^\beta) \sin^2 \Theta_k \sin^2 \Theta_{k+q}}{\hbar\omega + E_k^\beta - E_{k+q}^\beta} \\ & + \frac{(f_k^\beta - f_{k+q}^\alpha) \sin^2 \Theta_k \cos^2 \Theta_{k+q}}{\hbar\omega + E_k^\beta - E_{k+q}^\alpha} \\ & \left. + \frac{(f_k^\alpha - f_{k+q}^\beta) \cos^2 \Theta_k \sin^2 \Theta_{k+q}}{\hbar\omega + E_k^\alpha - E_{k+q}^\beta} \right], \quad (13) \end{aligned}$$

290

291 where f_k^α is the Fermi-Dirac distribution function for the k th
292 Bloch state of the α hybridized electronic band. The imagi-
293 nary part of the polarization part is given by

$$\begin{aligned} \text{Im } \Pi_q(\omega + i\eta) = & -\frac{2\pi\lambda_{q,\gamma}^2}{N} \sum_k [\delta(\hbar\omega + E_k^\alpha - E_{k+q}^\alpha)(f_k^\alpha \\ & - f_{k+q}^\alpha) \cos^2 \Theta_k \cos^2 \Theta_{k+q} + \delta(\hbar\omega + E_k^\beta \\ & - E_{k+q}^\beta)(f_k^\beta - f_{k+q}^\beta) \sin^2 \Theta_k \sin^2 \Theta_{k+q} + \delta(\hbar\omega \\ & + E_k^\beta - E_{k+q}^\alpha)(f_k^\beta - f_{k+q}^\alpha) \sin^2 \Theta_k \cos^2 \Theta_{k+q} \\ & + \delta(\hbar\omega + E_k^\alpha - E_{k+q}^\beta)(f_k^\alpha \\ & - f_{k+q}^\beta) \cos^2 \Theta_k \sin^2 \Theta_{k+q}]. \quad (14) \end{aligned}$$

300 The real part and imaginary part are connected by the
301 Kramers-Krönig relations

$$\text{Re } \Pi_q(\omega) = \frac{1}{\pi} \int_{-\infty}^{+\infty} d\omega' \frac{\text{Im } \Pi_q(\omega' + i\eta)}{\omega' - \omega} \quad (15)$$

302

303 and

which expresses causality. The polarization part satisfies
symmetry relations. In particular, due to time-reversal invari-
ance, the real part is an even function of ω and imaginary
part is an odd function of ω .

To lowest order in the electron-phonon interaction, the
renormalized phonon and decay rates frequencies are deter-
mined by the complex poles of the approximate phonon
propagator

$$D_q(\omega) = \frac{2\hbar\omega_q}{\hbar^2\omega^2 - \hbar^2\omega_q^2 - 2\hbar\omega_q\Pi_q(\omega)}, \quad (17)$$

which omits the couplings between the various phonon
modes. This yields the equation

$$\hbar^2\omega^2 - \hbar^2\omega_q^2 - 2\hbar\omega_q\Pi_q(\omega) = 0, \quad (18)$$

which is to be solved graphically. The real parts of the pho-
non frequencies are approximately given by the intersection
of the curves $\omega^2 - \omega_q^2$ and $2\omega_q \text{Re } \Pi_q(\omega)$, and the phonon
decay rates are given by $\text{Im } \Pi_q(\omega + i\eta)$ at the intersection.

The form of the frequency-dependent polarization part is
shown in Fig. 2 for the values of $q=(0,0,0)$ and q
 $=(\pi, \pi, \pi)$. For these particular q values, the intraband scat-
tering processes do not contribute to the polarization part in
the energy range of interest. The low-energy intraband contri-
butions are restricted to a range of small but finite q and
give rise to the structures seen in Fig. 3. The intraband contri-
butions are unlikely to yield phonon anomalies since one
expects that Fermi velocity will be much greater than the
speed of sound, so the Born-Oppenheimer approximation ap-
plies. For $q=(0,0,0)$ the intraband contributions to the po-
larization part vanish identically when $\omega \neq 0$ and the polar-
ization part, shown in the left panel of Fig. 2, is dominated
by the interband contributions. The interband processes ex-
hibits a sharp peak at the threshold energy of $2V$ which cor-
responds to the direct gap. Since $2V$ is much larger than the
phonon energy scale, the renormalizations of the phonon fre-
quencies are expected to be minimal at $q=(0,0,0)$. On the
other hand, for $q=(\pi, \pi, \pi)$ the threshold for the interband
excitations will be on the order of the much smaller indirect-
gap energy $\Delta=4V^2/W$, as can be seen in the right panel of
Fig. 2.

When the threshold for interband excitations is greater
than the bare phonon frequency, the polarization part has the
effect of reducing the phonon frequency. The softening in-
creases when the separation between the bare phonon fre-
quency and the indirect gap is reduced. When the threshold
energy is comparable to the optic phonon frequency, then the
low-energy electronic excitations can resonate with the optic
phonons leading to the formation of modes of mixed elec-
tronic and phononic character. In particular, for phonons with
bare frequencies slightly above the interband threshold, the
phonon spectral density may show two features: a narrow
feature with energies below the threshold and a broader
structure located above the threshold but below the bare pho-

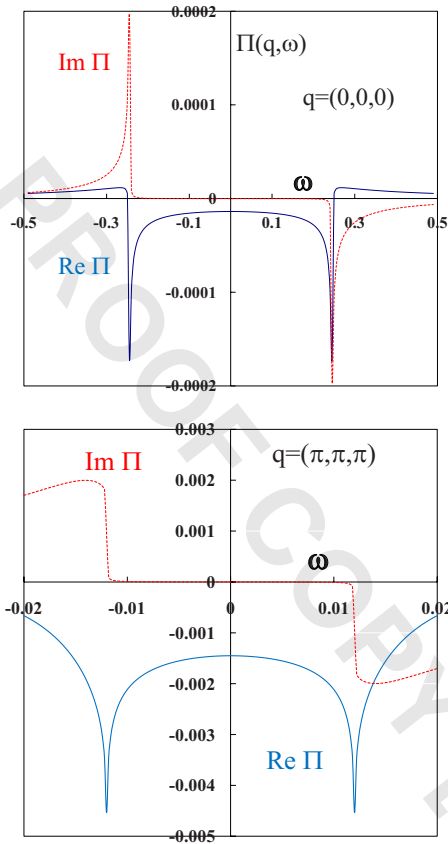


FIG. 2. (Color online) The left panel shows the frequency dependence of the polarization part for $q=(0,0,0)$. The real part is symmetric in frequency (solid blue line) and imaginary part is odd (dashed red line). The polarization part shows structure at the energy of the direct gap $2V$. The right panel shows the corresponding polarization part for $q=(\pi, \pi, \pi)$. The polarization part shows structure at the threshold for interband transitions. This threshold is related to the indirect gap Δ . The slight shift is caused by the chemical potential μ which is positioned at an energy of 6 meV in the upper hybridized band. Note the different scales in the two panels.

AQ:
#6

356 non frequency which represents the resonance. The graphical
357 solution and the phonon spectral density are shown in Fig. 4.
358 The ω -integrated intensity of the lower mode is given by the
359 expression

$$\left[1 - \frac{\partial}{\partial \hbar \omega} \Pi_q(\omega) \right]^{-1}, \quad (19)$$

360

361 which should be reduced below unity. The intrinsic width of
362 the mode due to anharmonic interactions (not considered
363 here) should be reduced by the same factor. The two solu-
364 tions may be designated as breathing modes which involve
365 the phonons coupling coherently with f - d charge fluctuations
366 and the concomitant change in ionic radii. The model shows
367 that this resonance should only occur for the higher fre-
368 quency optic modes, and then only for a limited range of
369 large q values for which the threshold energy for interband
370 electronic excitations is reduced below the bare phonon fre-
371 quency. This finding is qualitatively in agreement with the
372 experimentally results of Manley *et al.*¹⁵ which show that the

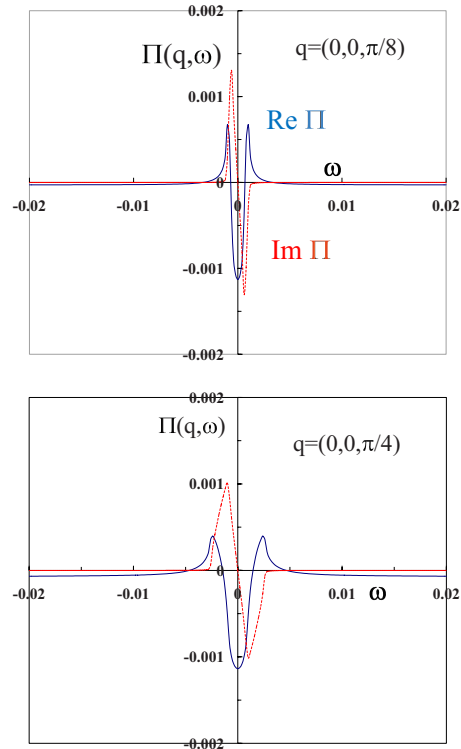


FIG. 3. (Color online) The left panel shows the low-frequency variation in the polarization part for $q=(0,0,\pi/8)$. The real part is symmetric in frequency (solid blue line) and imaginary part is odd (dashed red line). The right panel shows the corresponding polarization part for $q=(0,0,\pi/4)$. For this range of momenta and frequencies, the polarization part is dominated by the intraband contribution and resembles the Lindhardt function for electrons with renormalized masses.

new mode is found predominantly near the Y point at the
Brillouin-zone boundary. If the phonon frequency is further
increased above the electronic threshold, the high-energy
resonance may eventually turn into a bound state. For further
increases in the phonon frequency, the lower mode may rapidly
lose intensity and merge with the continuum. In such cases, the
lower mode has an energy ω below the indirect-gap energy Δ
which is approximately given by

$$\hbar \omega \approx \Delta \left(1 - \exp \left[- \frac{\Delta (\hbar^2 \omega_q^2 - \Delta^2)}{\lambda_q^2 \hbar \omega_q} \right] \right) \quad (20)$$

and the ω -integrated intensity should show an exponential
fall off. On further increase in the phonon frequency or
weakening of the electron-phonon interaction, the lower mode
may have a protracted existence as a narrow resonance as seen
in Fig. 5.

AQ
#5

IV. DISCUSSION

387

The major assumption of the above analysis is that there
exist low-energy electronic excitations which have energies
comparable to those of the optic phonon modes. Since the
electronic energy scales derived from first-principles
calculations³² at ambient conditions are about a factor of 10

392

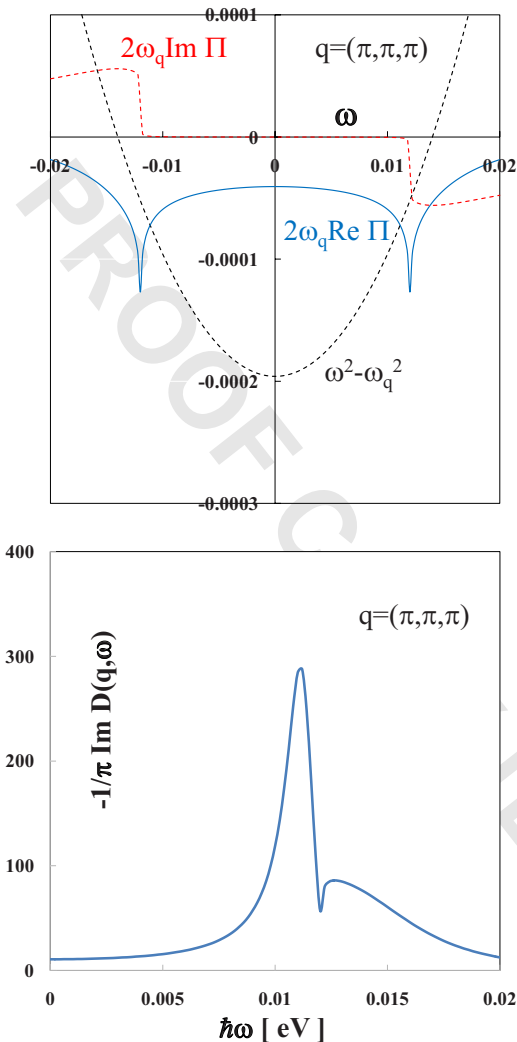


FIG. 4. (Color online) The left panel shows the graphical solution for the renormalized phonon frequency. The renormalized phonon frequency is given by the intersection of the line $2\omega_q \Pi_q(\omega)$ (solid blue line) with the parabola $\omega^2 - \omega_q^2$ (dashed black line). The plot shows that the renormalized phonon frequency exhibits a significant softening when the bare frequency is comparable to the threshold energy Δ . The right panel shows the phonon spectral density. It shows the softened phonon line at lower frequencies and the formation of resonance mode of mixed electron and phonon character at higher frequencies. A constant has been added to the phonon linewidths to simulate the contributions from anharmonic processes.

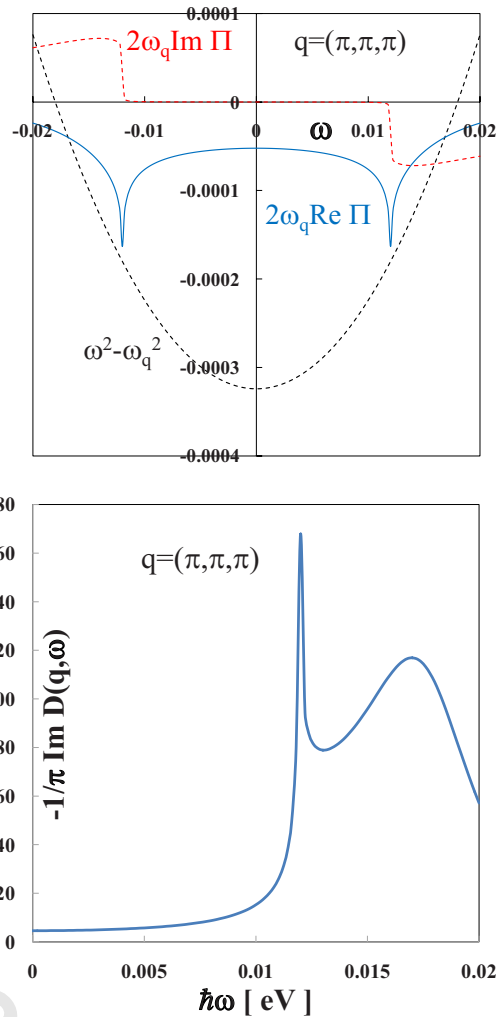


FIG. 5. (Color online) The left panel shows the graphical solution for the renormalized phonon frequency. This figure differs from Fig. 5 in that the value of the bare phonon frequency has been increased slightly. The renormalized phonon frequency is given by the intersection of the line $2\omega_q \Pi_q(\omega)$ (solid blue line) with the parabola $\omega^2 - \omega_q^2$ (dashed black line). The plot shows that although the renormalized phonon frequency lies above the threshold energy Δ , the separation of the curves still shows a local minimum near Δ which may allow the lower frequency mode to exist as a resonance. The right panel shows the phonon spectral density. It shows that in this case, a narrow resonance exists near the threshold energy. A constant has been added to the phonon linewidths to simulate the contributions from anharmonic processes.

393 larger than those required for the formation of the breathing
 394 mode, the postulated reduction requires a many-body expla-
 395 nation. One possibility is that the reduction in scale is due to
 396 the Kondo effect or low-energy valence fluctuations³⁹ as has
 397 been used⁴⁰ to predict the experimentally determined phonon
 398 anomalies in plutonium.⁴¹ A second possibility, namely, that
 399 the reduction is due to a polaronic effect is outlined below.
 400 The first occurrence of the split phonon modes at high
 401 temperatures can be understood if one assumes that the hy-
 402 bridization energy is subject to a polaronic reduction. This
 403 can be achieved by using a canonical transformation which is

a variant of the Lee-Low-Pines transformation⁴⁸ and is given 404
 by 405

$$\hat{U} = \exp \left[-\frac{1}{\sqrt{N}} \sum_{q,j,\sigma,\gamma} \frac{\lambda_{q,\gamma}}{\hbar \omega_{q,\gamma}} (a_{q,\gamma}^\dagger - a_{-q,\gamma}) f_{j,\sigma}^\dagger f_{j,\sigma} \exp(iq \cdot R_j) \right]. \quad (21) \quad 406$$

Applying the transformation to the parts of the Hamiltonian 407
 which couple to the phonons, one can eliminate the electron- 408
 phonon interaction since 409

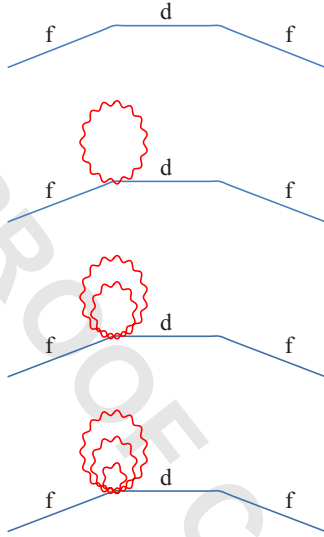


FIG. 6. (Color online) The series of simultaneous emission and absorption of phonons at a hybridization vertex which leads to a polaronic reduction in the hybridization matrix element. The solid blue lines represent the noninteracting one-electron Green's function and the red wavy lines represent the phonon propagators.

$$\begin{aligned} \hat{H}'_{ph} &= \hat{U}^\dagger \left[\sum_{q\gamma} \hbar\omega_{q\gamma} a_{q\gamma}^\dagger a_{q\gamma} + \frac{1}{\sqrt{N}} \sum_{q,k,\gamma} \lambda_{q\gamma} (a_{q\gamma}^\dagger + a_{-q\gamma}) f_{k\gamma}^\dagger f_{k-q} \right] \hat{U} \\ &= \sum_{q,\gamma} \hbar\omega_{q\gamma} a_{q\gamma}^\dagger a_{q\gamma} - \frac{1}{N} \sum_{q,k,k'} \frac{\lambda_{q\gamma}^2}{\hbar\omega_{q\gamma}} f_{k-q}^\dagger f_{k'+q}^\dagger f_{k'} \end{aligned} \quad (22)$$

Thus, the Hamiltonian is diagonal in the limit $V \rightarrow 0$ in which case, the linear electron-phonon coupling is removed but the process, produces a Frank-Condon shift of the f level and also produces an oscillatory long-ranged interaction between the f electrons.^{45,46} The canonical transformation has the effect of producing a dynamic renormalization of the hybridization term to yield

$$\begin{aligned} H'_V &= \sum_{j,k,\gamma} \left\{ V \exp[i\mathbf{k} \cdot \mathbf{R}_j] f_{j,\alpha}^\dagger d_{k,\alpha} \exp \left[-\frac{1}{\sqrt{N}} \sum_{q,\gamma} \frac{\lambda_{q,\gamma}}{\hbar\omega_{q,\gamma}} (a_{q,\gamma}^\dagger - a_{-q,\gamma}) \exp(i\mathbf{q} \cdot \mathbf{R}_j) \right] + \text{H.c.} \right\}. \end{aligned} \quad (23)$$

If this is replaced by the thermal average, as in the Gutzwiller approximate treatment of electronic correlations, one recovers a polaronic reduction in the effective hybridization interaction of the form

$$V \rightarrow \tilde{V} = V \exp \left\{ -\frac{1}{2N} \sum_{q,\gamma} \left(\frac{\lambda_{q,\gamma}}{\hbar\omega_{q,\gamma}} \right)^2 [1 + 2N(\omega_{q,\gamma})] \right\}. \quad (24)$$

Diagrammatically, this corresponds to the simultaneous emission and absorption of an indefinite number of phonons at the hybridization vertex, as indicated by the infinite series depicted in Fig. 6. The temperature dependence of the renor-

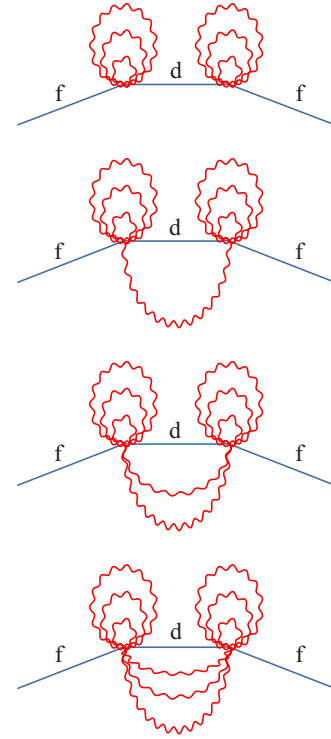


FIG. 7. (Color online) The self-energy for the f quasiparticle Green's function corresponding to the series of emission and absorption of phonons propagating between two adjacent polaronically renormalized hybridization vertices. The symbols are the same as in Fig. 6.

malized hybridization matrix element is similar to that found in Holstein's treatment of the small polaron.⁴⁹ It is hypothesized that the temperature-dependent renormalization of the hybridization matrix element, and the concomitant reduction in the indirect hybridization gap, is responsible for the occurrence of the breathing mode at high temperatures. This polaronic renormalization only occurs for the low-energy f quasiparticles. The higher energy excitations are unrenormalized, as is indicated below. For moderately large polaronic reductions, one might expect that the f -electron self-energy could be calculated to leading orders in \tilde{V}^2 , and that the dynamic part of the hybridization might also be expanded in powers of $(\frac{\lambda_{q,\gamma}}{\hbar\omega_{q,\gamma}})^2$. To lowest nontrivial order in the effective hybridization, the self-energy for the fermionic part of the transformed f electron Green's function can be expanded in powers of the dynamic electron-phonon coupling as depicted in Fig. 7. This yields the expression

$$\begin{aligned} \Sigma_f(\mathbf{k}, \omega) &\approx |\tilde{V}|^2 \left\{ \frac{1}{\hbar\omega - \epsilon_{\mathbf{k}} + \mu} \right. \\ &+ \frac{1}{N} \sum_{q,\gamma} \left(\frac{\lambda_{q,\gamma}}{\hbar\omega_{q,\gamma}} \right)^2 \left[\frac{1 + N(\omega_{q,\gamma}) - f_{\mathbf{k}-q}}{\hbar\omega - \epsilon_{\mathbf{k}-q} + \mu - \hbar\omega_{q,\gamma}} \right. \\ &\left. \left. + \frac{N(\omega_{q,\gamma}) + f_{\mathbf{k}-q}}{\hbar\omega - \epsilon_{\mathbf{k}-q} + \mu + \hbar\omega_{q,\gamma}} \right] + \dots \right\}. \end{aligned} \quad (25)$$

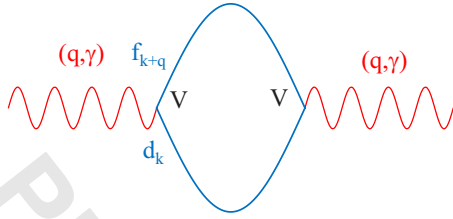


FIG. 8. (Color online) The lowest-order contribution to the phonon polarization part, in the transformed representation. For clarity, the polaronic renormalizations of the hybridization vertices \tilde{V} are not shown. The symbols are the same as in Fig. 6.

$$+ \left. \frac{(f_k^\alpha - f_{k+q}^\beta) \sin^2 \Theta_k \sin^2 \Theta_{k+q}}{\hbar \omega + E_k^\alpha - E_{k+q}^\beta} \right] \quad (28) \quad 475$$

in which all terms involve the polaronically renormalized 476 hybridization matrix element \tilde{V} . This has the same energetic 477 structure as that considered previously, although the intensities 478 differ. The polaronically renormalized indirect gap is expected 479 to decrease with increasing temperatures. Initially, it is 480 expected that this reduction will have the effect of producing 481 an increase in the magnitude of the polarization part 482 (evaluated at the bare phonon frequency) as the temperature 483 increases. This results in an initial softening of the optic 484 phonon modes with increasing temperature, consistent with 485 the experimental findings of Manley *et al.*¹³ The polaronic 486 reduction in the indirect gap also yields the result that the 487 breathing modes only forms at sufficiently high temperatures, 488 at which the indirect gap becomes comparable to the optic 489 phonon energy. Furthermore, these breathing modes are only 490 expected to exist over a limited range of temperatures 491 since for sufficiently high temperatures the effective strength 492 of the electron-phonon coupling interaction given by 493

450 The first term in the above expansion produces a highly 451 renormalized branch of quasiparticle excitations close to the 452 Fermi energy. However, at excitation energies greater than 453 $\hbar \omega_D$ from the Fermi surface, the quasiparticle excitations 454 becomes unrenormalized as can be inferred by expanding the 455 second and third terms in powers of $\omega_{q\gamma}$, yielding

$$456 \quad \Sigma_f(k, \omega) \approx |\tilde{V}|^2 \left\{ \frac{1}{\hbar \omega - \epsilon_k + \mu} \right. \\ 457 \quad + \frac{1}{N} \sum_{q,\gamma} \left(\frac{\lambda_{q,\gamma}}{\hbar \omega_{q,\gamma}} \right)^2 \left[\frac{1 + 2N(\omega_{q,\gamma})}{\hbar \omega - \epsilon_{k-q} + \mu} \right] \\ 458 \quad + \frac{1}{N} \sum_{q,\gamma} \left(\frac{\lambda_{q,\gamma}}{\hbar \omega_{q,\gamma}} \right)^2 \hbar \omega_{q,\gamma} \left[\frac{1 - 2f_{k-q}}{(\hbar \omega - \epsilon_{k-q} + \mu)^2} \right] \\ 459 \quad \left. + \dots \right\}. \quad (26)$$

460 For energies removed from the Fermi energy (so the denomi- 461 nators are far from resonance), it can be inferred that the 462 second term represents the lowest-order term of the series 463 which has the effect of removing the polaronic reduction in 464 the square of the effective hybridization matrix elements

$$465 \quad |\tilde{V}|^2 \approx |V|^2 \exp \left\{ - \frac{1}{N} \sum_{q,\gamma} \left(\frac{\lambda_{q,\gamma}}{\hbar \omega_{q,\gamma}} \right)^2 [1 + 2N(\omega_{q,\gamma})] \right\} \times \left\{ 1 \right. \\ 466 \quad \left. + \frac{1}{N} \sum_{q,\gamma} \left(\frac{\lambda_{q,\gamma}}{\hbar \omega_{q,\gamma}} \right)^2 [1 + 2N(\omega_{q,\gamma})] + \dots \right\}. \quad (27)$$

467 This leads to the overall f density of states being unrenor- 468 malized by the electron-phonon coupling.

469 The low-energy contribution to the irreducible polariza- 470 tion part is given by the quasiparticle contribution shown in 471 Fig. 8, which has the leading-order contribution given by

$$472 \quad \Pi_q(\omega) = \frac{2}{N} \left(\frac{\tilde{V} \lambda_{q,\gamma}}{\hbar \omega_{q,\gamma}} \right)^2 \sum_k \left[\frac{(f_k^\alpha - f_{k+q}^\alpha) \sin^2 \Theta_k \cos^2 \Theta_{k+q}}{\hbar \omega + E_k^\alpha - E_{k+q}^\alpha} \right. \\ 473 \quad + \frac{(f_k^\beta - f_{k+q}^\beta) \cos^2 \Theta_k \sin^2 \Theta_{k+q}}{\hbar \omega + E_k^\beta - E_{k+q}^\beta} \\ 474 \quad \left. + \frac{(f_k^\beta - f_{k+q}^\alpha) \cos^2 \Theta_k \cos^2 \Theta_{k+q}}{\hbar \omega + E_k^\beta - E_{k+q}^\alpha} \right]$$

$$\frac{\tilde{V} \lambda_{q,\gamma}}{\hbar \omega_{q,\gamma}} \quad (29) \quad 494$$

will be reduced below the critical strength necessary to cause 495 the resonance to split the modes. 496

In summary, we have presented a model to describe the 497 phonon anomalies in α -uranium that is an alternative to the 498 intrinsically localized mode description. In particular, we 499 have shown that when the f - d electronic excitation energies 500 are comparable to the optic phonon frequencies, strong 501 f -electron-phonon coupling can cause the phonon frequen- 502 cies to soften and in a critical range may cause the phonon 503 modes to become resonant and split forming breathing 504 modes of mixed electron-phonon characters. These modes 505 will only occur for a limited range of q values and are res- 506 tricted to the higher energy portions of the unrenormalized 507 phonon spectra. Furthermore, we have indicated how the ob- 508 served temperature-dependent softening of the optic phonon 509 frequencies and the evolution of the new mode can be rec- 510 onciled with this theory, if one assumes the existence of a 511 significant polaronic renormalization of the quasiparticle ex- 512 citations. 513

ACKNOWLEDGMENTS 514

This work was supported by a grant from the U.S. Depart- 515 ment of Energy, Office of Basic Energy Sciences through 516 Award No. DEFG02-84ER45872. The authors would also 517 like to acknowledge stimulating conversations with G. H. 518 Lander, J. C. Lashley, M. E. Manley, J. L. Smith, and J. 519 Tobin. 520

- 521 ¹G. H. Lander, E. S. Fisher, and S. D. Bader, *Adv. Phys.* **43**, 1
522 (1994).
- 523 ²W. P. Crummett, H. G. Smith, R. M. Nicklow, and N. Wakabayashi, *Phys. Rev. B* **19**, 6028 (1979).
- 524 ³W. Kohn, *Phys. Rev. Lett.* **2**, 393 (1959).
- 525 ⁴H. G. Smith, N. Wakabayashi, W. P. Crummett, R. M. Nicklow,
526 G. H. Lander, and E. S. Fisher, *Phys. Rev. Lett.* **44**, 1612
527 (1980).
- 528 ⁵G. H. Lander, E. S. Fisher, N. Wakabayashi, W. P. Crummett,
529 and R. M. Nicklow, *Physica B & C* **102**, 326 (1980).
- 530 ⁶Y. Yamada, *Phys. Rev. B* **47**, 5614 (1993).
- 531 ⁷J. C. Marmeggi, R. Currat, A. Bouvet, and G. H. Lander, *Physica*
532 *B* **263-264**, 624 (1999).
- 533 ⁸L. Fast, O. Eriksson, B. Johansson, J. M. Wills, G. Straub, H.
534 Roeder, and L. Nordstrom, *Phys. Rev. Lett.* **81**, 2978 (1998).
- 535 ⁹J. Bouchet, *Phys. Rev. B* **77**, 024113 (2008).
- 536 ¹⁰J. C. Marmeggi, R. Currat, A. Bouvet, and G. H. Lander, *Physica*
537 *B* **276-278**, 272 (2000).
- 538 ¹¹C. S. Barrett, M. H. Mueller, and R. L. Hitterman, *Phys. Rev.*
539 *B* **129**, 625 (1963).
- 540 ¹²J. W. Ross and D. J. Lam, *Phys. Rev.* **165**, 617 (1968).
- 541 ¹³M. E. Manley, B. Fultz, R. J. McQueeney, C. M. Brown, W. L.
542 Hulst, J. L. Smith, D. J. Thoma, R. Osborn, and J. L. Robertson,
543 *Phys. Rev. Lett.* **86**, 3076 (2001).
- 544 ¹⁴M. E. Manley, G. H. Lander, H. Sinn, A. Alatas, W. L. Hulst, R.
545 J. McQueeney, J. L. Smith, and J. Willit, *Phys. Rev. B* **67**,
546 052302 (2003).
- 547 ¹⁵M. E. Manley, M. Yethiraj, H. Sinn, H. M. Volz, A. Alatas, J. C.
548 Lashley, W. L. Hulst, G. H. Lander, and J. L. Smith, *Phys. Rev.*
549 *Lett.* **96**, 125501 (2006).
- 550 ¹⁶M. E. Manley, J. W. Lynn, Y. Chen, and G. H. Lander, *Phys.*
551 *Rev. B* **77**, 052301 (2008).
- 552 ¹⁷E. Fermi, J. Pasta, and S. Ulam, ■ Report No. LA-1940, May
553 1955 (unpublished).
- AQ: #54 ¹⁸D. J. Korteweg and F. de Vries, *Philos. Mag.* **39**, 422 (1895).
- 554 ¹⁹C. S. Gardner, J. M. Greene, M. D. Kruskal, and R. M. Muira,
555 *Phys. Rev. Lett.* **19**, 1095 (1967).
- 8 ²⁰M. Toda, *J. Phys. Soc. Jpn.* **22**, 431 (1967); M. Toda and M.
556 Wati, *ibid.* **34**, 18 (1973).
- AQ: #58 ²¹S. Flach, *Phys. Rev. E* **50**, 3134 (1994).
- 9 ²²G. H. Derrick, *J. Math. Phys.* **5**, 1252 (1964).
- 557 ²³K. M. Leung, D. W. Hone, D. L. Mills, P. S. Riseborough, and S.
558 E. Trullinger, *Phys. Rev. B* **21**, 4017 (1980).
- 559 ²⁴P. S. Riseborough and S. E. Trullinger, *Phys. Rev. B* **22**, 4389
560 (1980).
- 561 ²⁵M. E. Manley, A. J. Sievers, J. W. Lynn, S. A. Kiselev, N. I.
562 Agladze, Y. Chen, A. Llobet, and A. Alatas, *Phys. Rev. B* **79**,
563 134304 (2009).
- 564 ²⁶S. A. Kiselev and A. J. Sievers, *Phys. Rev. B* **55**, 5755 (1997).
- 565 ²⁷M. E. Manley, *Acta Mater.* **58**, 2926 (2010).
- 566 ²⁸H. L. Skriver and I. Mertig, *Phys. Rev. B* **32**, 4431 (1985).
- 567 ²⁹J. M. Wills and O. Eriksson, *Phys. Rev. B* **45**, 13879 (1992).
- ³⁰C. P. Opeil, R. K. Schulze, M. E. Manley, J. C. Lashley, W. L.
Hulst, R. J. Hanrahan, Jr., J. L. Smith, B. Mihaila, K. B. Blago-
goev, R. C. Albers, and P. B. Littlewood, *Phys. Rev. B* **73**,
165109 (2006).
- ³¹D. Graf, R. Stillwell, T. P. Murphy, J.-H. Park, M. Kano, E. C.
Palm, P. Schlottmann, J. Bourg, K. N. Collar, J. C. Cooley, J. C.
Lashley, J. Willit, and S. W. Tozer, *Phys. Rev. B* **80**, 241101
(2009).
- ³²A. N. Chantis, R. C. Albers, M. D. Jones, M. van Schilfgaarde,
and T. Kotani, *Phys. Rev. B* **78**, 081101 (2008).
- ³³A. Hjelm, O. Eriksson, and B. Johansson, *Phys. Rev. Lett.* **71**,
1459 (1993).
- ³⁴N. Stojić, J. W. Davenport, M. Komelj, and J. Glimm, *Phys. Rev.*
B **68**, 094407 (2003).
- ³⁵G. Schadler, P. Weinberger, A. M. Boring, and R. C. Albers,
Phys. Rev. B **34**, 713 (1986).
- ³⁶I. V. Solov'yev, A. I. Liechtenstein, V. A. Gubanov, V. P.
Antropov, and O. K. Andersen, *Phys. Rev. B* **43**, 14414 (1991).
- ³⁷J. C. Lashley, A. Lawson, R. J. McQueeney, and G. H. Lander,
Phys. Rev. B **72**, 054416 (2005).
- ³⁸P. Söderlind, *Europhys. Lett.* **55**, 525 (2001).
- ³⁹S. Y. Savrasov, G. Kotliar, and E. Abrahams, *Nature (London)*
410, 793 (2001).
- ⁴⁰X. Dai, S. Y. Savrasov, G. Kotliar, A. Migliori, H. Ledbetter, and
E. Abrahams, *Science* **300**, 953 (2003).
- ⁴¹J. Wong, M. Krisch, D. L. Farber, F. Occelli, A. J. Schwartz,
T.-C. Chiang, M. Wall, C. Boro, and R. Xu, *Science* **301**, 1078
(2003).
- ⁴²K. S. Moore and G. van der Laan, *Rev. Mod. Phys.* **81**, 235
(2009).
- ⁴³P. Entel, N. Grewe, and H. J. Leder, *Zeit. für Physik B* **30**, 393
(1978).
- ⁴⁴P. S. Riseborough and X. Yang, *J. Magn. Magn. Mater.* **310**, 938
(2007).
- ⁴⁵D. S. Sherrington and P. S. Riseborough, *J. Phys. C* **4**, 255
(1976).
- ⁴⁶D. S. Sherrington and S. von Molnar, *Solid State Commun.* **16**,
1347 (1975).
- ⁴⁷J. Bardeen and D. Pines, *Phys. Rev.* **99**, 1140 (1955).
- ⁴⁸T. D. Lee, F. E. Low, and D. Pines, *Phys. Rev.* **90**, 297 (1953).
- ⁴⁹T. Holstein, *Ann. Phys. (N.Y.)* **8**, 325 (1959) **8**, 343 (1959).

AUTHOR QUERIES —

- #1 Au: Please provide the complete address for the affiliation.
- #2 Au: Phys. Rev. prefers not to publish claims of novelty or priority. Please refer to memo Policy Note New/Novel. To access this memo, please click on the 'Production Memos for Authors' link which is located on the Important Notice Instructions, above the Download button for proof of forthcoming article.
- #3 Au: Phys. Rev. prefers not to publish claims of novelty or priority. Please refer to memo Policy Note New/Novel. To access this memo, please click on the 'Production Memos for Authors' link which is located on the Important Notice Instructions, above the Download button for proof of forthcoming article.
- #4 Au: Phys. Rev. prefers not to publish claims of novelty or priority. Please refer to memo Policy Note New/Novel.
- #5 Au: Please verify the insertion of the citation of Fig. 5 in text.
- #6 Au: Although a caption makes reference to color online, figures will appear black and white in print. Please make sure the caption make sense to print reader.
- #7 Au: Please provide name of institute in Ref. 17.
- #8 Please verify contents of Ref. 18
- #9 Au: Please verify the year in Ref. 20.
- #10 Au: Please verify the first author in Ref. 34.
- #11 Au: Please provide the full journal title, the coden, and/or ISSN for the journal in Ref. 43.
- #12 Please verify contents of Ref. 46